Templated wide band-gap nanostructures

A. Alizadeh,[a] P. Sharma,[b] S. Ganti, S. F. LeBoeuf, and L. Tsakalakos
General Electric, Global Research Center, Niskayuna, New York 12309

(Received 12 January 2004; accepted 12 March 2004)

In this two-pronged work we report (a) a study of defect nucleation in three-dimensional confined nanoislands and (b) a surface-elasticity induced size effect in the optoelectronic properties of embedded and templated semiconducting nanostructures. Several key features in the design of nanostructure templates are analyzed and dislocation free contour maps are presented for combination of various lattice mismatches, substrates, and geometrical dimensions. Unlike the case for thin epitaxial films, it is found that for nanostructures, below a certain critical lateral dimension, dislocation free structures of *any* thickness can be grown. With regards to the optoelectronic properties of nanostructures, while size dependency due to quantum confinement and electrostatic interactions are well known, we show that an additional *size-dependent strain* is caused by the distinct elastic behavior of surfaces and interfaces at the nanoscopic scale compared to the macroscopic scale. This is in contrast to the usual way strain is linked to optoelectronic properties, i.e., via classical elasticity, which ignores surface energies and is intrinsically *size independent*. Surface strains appear to be only influential in the nanometer regime due to appreciable surface-to-volume ratios. Among our major conclusions are that errors as large as 100 meV in band-gap prediction can incur if this size-dependent surface effect is ignored. © *2004 American Institute of Physics.* [DOI: 10.1063/1.1737477]

I. INTRODUCTION

Recently, semiconductor nanostructures (quantum dots and nanowires) have been the focus of intense research due to their intriguing optoelectronic properties.[1,2] With the advent of nanotechnology, there is a growing consensus in the technical community regarding the enormous application potential of wide band-gap (WBG) semiconductor nanostructures.[3–5] For instance, extremely low threshold laser diodes are feasible from nanostructured WBG materials, due to an increase in their nonlinear response with size reduction. Disappearance of the temperature dependent broadening behavior in quantum dot lasers as a consequence of electronic state confinement has also been reported.[3] In addition, WBG nanostructures have been recognized as the key components of light-emitting-diodes (LED) devices.[6] In the active region of conventional LED devices, e.g., InGaN quantum wells, it has been suggested that nanometer-scale compositional fluctuations of indium lead to ''quantum-dot-like'' states that suppress nonradiative recombination processes effectively.[7,8] Unfortunately, these compositional fluctuations and the resulting nanostructures that are formed from natural processes (such as self-assembly) exhibit a broad size and composition distributions. Consequently, the emission spectra of these LED devices are broadened and internal quantum efficiencies are severely limited by size disorder and spatial nonuniformity. In order to achieve the predicted performance of quantum dot based devices, it is necessary to engineer well-controlled *uniform size and composition* WBG nanostructures.

Recently, approaches have been proposed to grow WBG nanostructures.[9–11] Nanometer sized WBG quantum dots/wells have been generated using direct writing (exposure/liftoff) techniques.[12,13] However, nonradiative defects are produced during these procedures that severely compromise the material quality and its further use in optoelectronic devices. Self-assembled WBG quantum dots have been generated on a variety of substrates, where in some instances the growth process is assisted with a surfactant layer.[14–17] The self-assembly based techniques are relatively simple and yield high throughput, however, as mentioned earlier, the resulting WBG nanostructures often exhibit large morphological variabilities over the substrate. Recently, selective growth of extremely uniform WBG quantum dots has been reported by several authors.[18,19] Quantum dot fabrication through selective growth process consists of deposition of a thin SiO_2 layer on a substrate and its subsequent patterning with submicron holes; WBG nanostructures are then selectively grown inside the holes using a variety of techniques, such as metalorganic vapor deposition and molecular beam epitaxy. Lateral dimensions of the WBG nanostructures during this process are primarily controlled by the size of the holes in the SiO_2 mask.

Presently, it appears that the templated growth method is perhaps one of the more promising avenues for fabrication of tailored WBG nanostructures. Selective (or templated) growth of WBG nanostructures allows for a precise control over quantum dot size and location, and avoids the nonradiative defects associated with the direct writing techniques.[3] Most of the related research in the literature[18,19] has focused

[a]Author to whom correspondence should be addressed; electronic mail: alizadeh@crd.ge.com
[b]Permanent address: Department of Mechanical Engineering, University of Houston, Houston, TX 42015.

on the fabrication and synthesis of the WBG nanoislands inside the holes, while the impact of template design on the defect generation and optoelectronic properties of the nanostructures has received, comparatively, lesser attention. In the present work, we discuss various considerations for an optimum design of the nanotemplates. In particular, we address the following topics:

(1) Influence of substrate/template materials characteristics and dimensions on the misfit dislocation density of WBG nanostructures: We will show that for critical nanotemplate dimensions (usually below 100 nm), dislocation free wide band-gap nanostructures can be generated on highly mismatched substrates.

(2) Influence of substrate/template materials properties and dimensions on the band gap of WBG nanostructures: While the effects of strain on band gap are reasonably well understood, in the present work we show that proper accounting for surface energies and surface elasticity provides an extra size-dependent strain contribution that is typically neglected in classical elasticity on which most strain calculations and the consequent band structure calculations are based. In the nanometer regime, neglect of the surface elasticity effects leads to significant errors in the band-gap prediction of WBG nanostructures.

The article is organized as follows: In Sec. II, defect nucleation in 3D nanostructures is discussed and some technologically relevant numerical results are presented. In Sec. III, we elucidate the size-dependent surface elasticity strain mechanism on both embedded and templated quantum dots. Numerical results, physical insights and their implications are discussed in Sec. III followed by our main conclusions and a summary in Sec. IV.

II. MISFIT DISLOCATIONS IN WIDE BAND-GAP NANOSTRUCTURES

Most epitaxial fabrication methods result in the formation of misfit dislocations (MD) at the interface of the concerned semiconductor nanoisland (3D) or thin film (2D) and the substrate due to thermal and/or lattice mismatch induced strain.[20,21] For film thicknesses less than a certain critical value (often termed the critical film thickness h_c), the strain accommodation is entirely elastic. Beyond this critical thickness strain relaxation becomes energetically more favorable via introduction of misfit dislocations at the mismatched film–substrate interface. The classical Matthews–Blakeslee (MB) formula is frequently used for the calculation of the aforementioned critical thickness. Using an in-plane dislocation density, $\sqrt{\rho}|\mathbf{b}|$ on each side rather than a linear array of $\rho|\mathbf{b}|$, the Matthews–Blakelee (MB) formula can be expressed as:

$$\rho = 0, \quad h \leqslant h_c$$
$$\rho \cong \left(\frac{\epsilon^m}{|\mathbf{b}|}\right)^2 \cdot \left(1 - \frac{h_c}{h}\right)^2, \quad h > h_c, \tag{1}$$

where ρ is the dislocation density per unit area, $\mathbf{b}$ is the Burgers vector, h is the film thickness, and h_c is the critical thickness. The lattice mismatch strain represented by ϵ^m is given as $2(a_f - a_s)/(a_f + a_s)$ where a_f and a_s are the lattice parameters of the film and the substrate, respectively. The simple formula in Eq. (1) holds only for thin films, where stresses are nearly uniform. For 3D confined structures, MB formulation must be suitably modified to incorporate both the varying stress state of the confined structure, which becomes highly nonuniform, as well as dislocation energetics in a finite volume. Most of the previous works on confined geometries have focused on the laterally confined case, i.e., two-dimensional (2D) systems.[20,22–26] Three-dimensional confinement of nanoislands, which has not been sufficiently addressed in previous works, is the focus of the present work. In particular, we will focus on the following topics: (1) the variation of stresses in 3D confined structures as compared to thin film or the 2D case; (2) the effect of confinement in all directions on the dislocation density as compared to the thin film case; (3) the effect of passivation (template) material on the dislocation density of confined 3D nanostructures.

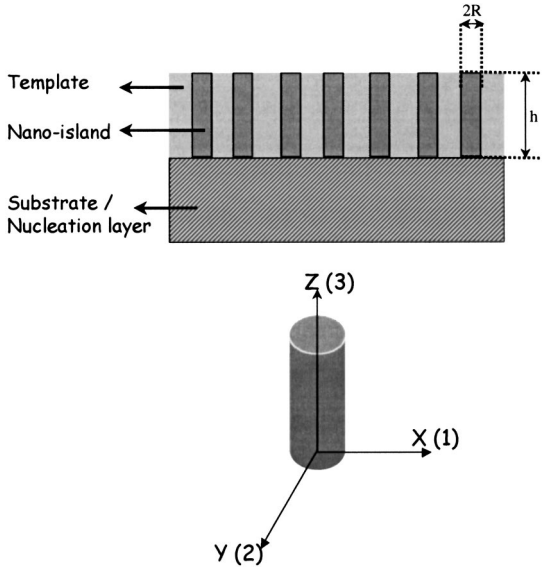

FIG. 1. Schematic of templated wide band-gap nanoisland.

A. Formulation

Consider the nanoisland geometry depicted in Fig. 1. For now it is assumed that the passivation constraining the nanoisland is either weak or nonexistent, such that no significant tractions are transmitted across the passivation and nanoisland interface. From a physical standpoint, small nanoislands will accommodate the lattice mismatch induced misfit strain through the stored elastic energy. Introduction of a single dislocation will become feasible only when such an event is energetically favorable. Assume that a single dislocation is introduced along the film–substrate interface. The change in energy upon introduction of a single dislocation along the z axis can be written as:

$$\Delta W = E_d - \int_0^h \sigma_{1j}(\mathbf{x}) b_j dz, \tag{2}$$

where E_d is the self-energy of a dislocation while σ is the

stress tensor, and b_j is the j component of the Burgers vector. Following Atkinson *et al.*,[24] we can rewrite Eq. (2) in terms of stress averages:

$$\Delta W = E_d - h\overline{\sigma}_{1i}(\mathbf{x})b_i, \tag{3}$$

where the overhead bar indicates spatial averaging with respect to the z coordinate. Dislocation nucleation is energetically unfavorable for $\Delta W > 0$ while for $\Delta W < 0$, system energy is lowered and hence the dislocation, if formed, remains stable.

1. Stress calculations

In subsequent calculations, it is assumed that the dislocation nucleation occurs along the interface of $[0,0,z]$ line. Since the average stresses are the highest at the center, this assumption has the effect that the calculated dislocation density will be larger than the true dislocation density. In other words, our prediction will be conservative, as is often desirable for engineering purposes.

Earlier reports of stress analysis in 2D confined structures by Luryi and Suhir were based on analytical calculations.[27] However, the accuracy of these empirical solutions become questionable for aspect ratios, h/R, larger than 0.2.[24] Again, for rectangular stripes, Faux *et al.* used Fourier analysis to construct the stress state analytically, however, in the three-dimensional context such an effort is extremely tedious.[25] In contrast, the finite element method can provide accurate results for the stress state in mismatched nanoislands. The average stress at $[0,0,z]$ is written as:

$$\langle \sigma_{11} \rangle = g\left(\frac{h}{R}\right)\sigma_{\text{thin film}} = k\epsilon^m g\left(\frac{h}{R}\right), \tag{4a}$$

where k is the biaxial modulus, which serves as a normalizing constant: $[k = 2\mu(1+\upsilon)/(1-\upsilon)]$. μ and ν are the Lame constant and the Poisson ratio, respectively. The expression for $g(h/R)$ is empirically fit to:

$$g(h/R) = \frac{1}{\alpha(h/R)}(1 - e^{-\alpha(h/R)}). \tag{4b}$$

The intrinsic size independency of classical elasticity ensures that $g(h/R)$ depends only on the nanoisland aspect ratio. The coefficient α depends primarily on the moduli of the nanoisland and the substrate and weakly on the Poisson's ratio of the two materials. Clearly, for vanishing aspect ratios, i.e., $h/R \to 0$, $g(h/R) \to 1$, and hence the stresses in Eq. (4a) degenerate to the classical thin film stress ($k\epsilon^m$). A commercially available finite element procedure (ABAQUS) is employed to investigate the stress state in the nanoislands numerically. Four-noded isoparametric axisymmetric elements are used in conjunction with isotropic material behavior for the nanoislands and the substrate. The function $g(h/R)$ is calculated by numerical averaging of the stresses along the z axis. The results are plotted in Fig. 2 for two different ratios of nanostructured semiconductor/substrate moduli.

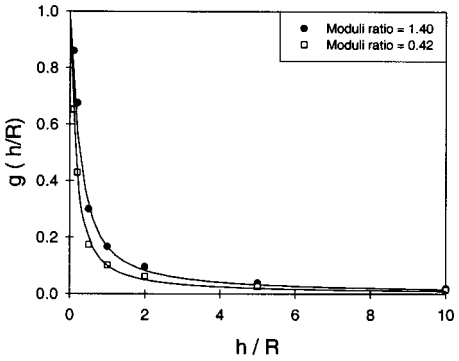

FIG. 2. Normalized stress function, $g(h/R)$ for two different compliance (moduli) ratios.

2. Dislocation energy calculations

In contrast to the thin-film case, i.e., $h/R \to 0$, the dislocation self-energy is altered in confined regions due to the presence of free boundaries, which impose the boundary conditions of zero tractions. In this work, we essentially adopt the formulation of Atkinson *et al.*[22–24] with minor modifications. These authors rigorously modeled the interaction energy of dislocations in 2D stripes with free surfaces. In this report, dislocation energetics for the 3D nanoislands were formulated using superposition on the 2D dislocation energy model of Atkinson *et al.* for a rectangular stripe. The expression for dislocation energy in the nanoislands is:

$$E_d = E_{d,\infty} + \sum_{n=1}^{\infty} E_I(4Rn) - E_I[(2n-1)2R]. \tag{5}$$

The term $E_{d,\infty}$ is simply the self-energy of the dislocation in an infinite medium while the interaction energy E_I can be calculated from the following expression:

$$\begin{aligned} E_I[d] = {} & \frac{\mu b_1^2}{4\pi(1-\nu)}\left(\ln(4a^2+1) + 4a^2\frac{4a^2+3}{(4a^2+1)^2}\right) \\ & + \frac{\mu b_2^2}{4\pi(1-\nu)}\left(\ln(4a^2+1) - 4a^2\frac{12a^2+1}{(4a^2+1)^2}\right) \\ & + \frac{\mu b_3^2}{4\pi}\ln(4a^2+1), \end{aligned} \tag{6}$$

where $a = h/d$, where d is the distance between image dislocations. Only edge dislocations parallel to the interface are considered. The infinite series in Eq. (5) converges rapidly and can be efficiently approximated. Substituting Eq. (5) in Eq. (3), the critical thickness h_c for dislocation nucleation can be expressed as:

$$h_c(R) = \frac{E_d(h_c/R)}{kb\epsilon^m g(h_c/R)}. \tag{7}$$

This equation has to be solved self-consistently. In particular, we note that the results are not only a function of the nanoisland aspect ratio but also its radius. To compute the finite dislocation density at dimensions beyond the critical ones, let a square array of dislocations be introduced in the nanoisland to relax the lattice mismatch induced strain. Then, in aver-

age, the mismatch strain is relaxed by an amount $\sqrt{\rho}|\mathbf{b}|$. Rearranging the terms in Eq. (7), we can write:

$$\epsilon^m - \sqrt{\rho(h/R,h)}|\mathbf{b}| = \frac{E_d(h/R)}{khbg(h/R)}$$

$$\Rightarrow \rho(h/R,h) = \left(\frac{\epsilon^m}{b}\right)^2 \left(1 - P_d P_s \frac{h_c}{h}\right)^2, \quad (8)$$

where we have introduced two nondimensional parameters, P_d and P_s:

$$P_d = \frac{E_d(h/R)}{E_d(h_c/R)}$$

$$P_s = \frac{g(h_c/R)}{g(h/R)}. \quad (9)$$

Equation (8) replaces the MB formula for 3D confined structures. Both the nondimensional parameters P_d and $P_s \rightarrow 1$ for $h/R \rightarrow 0$, and thus Eq. (8) degenerates to the classical formula for a thin film in the asymptotic limit. For finite values of h/R, however, Eq. (8) indicates reduced dislocation density.

B. Numerical results and discussion

We first present numerical results for the case where the bonding between passivation and the nanoislands is either weak or nonexistent. Such an assumption will be relaxed later, and the impact of passivation on the nanoisland stress state will be analyzed. Incidentally, note that one of the more commonly employed templates/passivation is SiO_2, which bonds very weakly, if at all, with the WBG nanostructure. Equation (7) can be used to develop dislocation free contours as a function of nanoisland dimensions (cylinder radius) and lattice mismatch. Figures 3(a) and 3(b) summarize dislocation free contours for various lattice mismatches and substrate compliances. For a given compliance ratio and lattice mismatch, each curve represents a locus of nanostructure dimensions below which no dislocations are nucleated. For large nanoisland radii, the dislocation free contours asymptotically converge to the thin film limit solution. However, for smaller nanoisland radii, significant deviations from the 2D thin film are observed. Below a critical radius, R_c, dislocation free contours are dominated by three-dimensional confinement effects. Figure 4 shows a typical dislocation free contour ($\Delta\epsilon = 1.69\%$), where the asymptotes of the thin film and 3D confined limits intersect at the critical radius R_c. Below R_c, dislocation free nanoislands can be grown to *any* thickness. Contrast it with the thin film case, where the critical thickness as predicted by the MB criteria is only a few nanometers. For instance, the critical thickness for GaN thin films grown on an AlN nucleation layer ($\Delta\epsilon = 2.7\%$) is about 2–3 nm.[28] Figure 5 shows the variation of R_c as a function of lattice mismatch for two different ratios of nanoislands/substrate moduli. As expected, R_c decreases monotonically as a function of lattice mismatch. Our results suggest that confinement dramatically reduces the dislocation density even for large values of $\Delta\epsilon$ (for instance 5%). Recently, Tu *et al.*[29] have shown that gallium nitride pillars (vertical nanorods) with lateral dimensions <12 nm are dislocation free. These experimental results appear to provide anecdotal evidence of the theoretical predictions presented in this article.

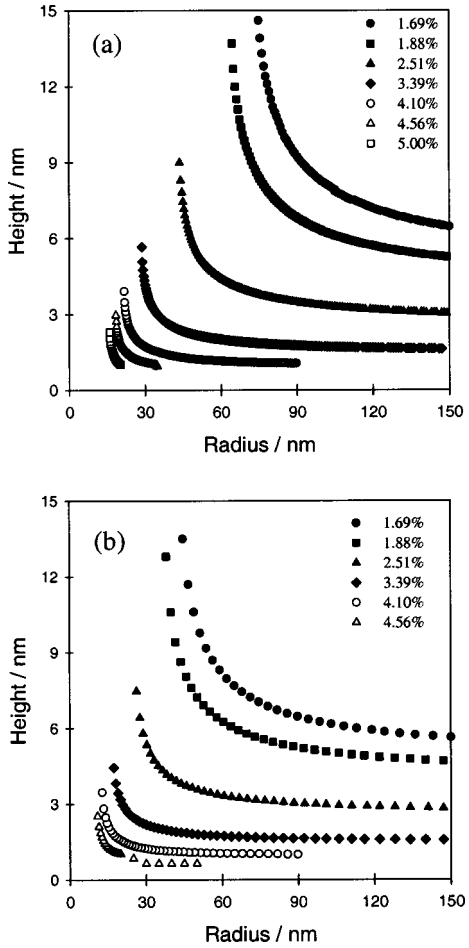

FIG. 3. Dislocation free contour maps for different lattice mismatches (a) ratio of moduli=1.40, (b) ratio of moduli=0.42.

As indicated earlier, the preceding results were predicted on the assumption of a nonexistent or weakly bonded passivation. The impact of passivation–nanoisland bonding is to impart tractions across the interface, thus changing the stress state in the nanoisland. The impact of these tractions are studied through variation in $g(h/R)$ for different passivation moduli. Figure 6 shows the effects of passivation for a

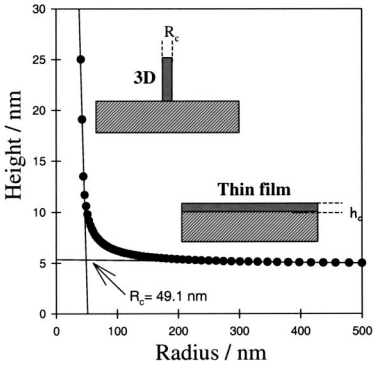

FIG. 4. Typical dislocation free contour curve, delineating two different regimes; 3D confined vs thin film.

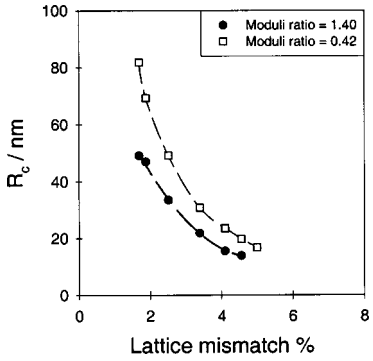

FIG. 5. Variation of critical radius vs lattice mismatch for two different compliance ratios.

nanoisland with an aspect ratio of $h/R=5$. Low values of passivation modulus imply low traction at the interface while a high value would constrain the nanoisland. For the specified aspect ratio of $h/R=5$, in the case when passivation bonding is either absent or very weak, the numerical value of $g(h/R)$ is small ~ 0.064. Intuitively, absence of passivation is recommended as it provides traction free surface for the nanoisland. A perhaps not so intuitive result is that a fairly rigid passivation and strong nanoisland–passivation bonding case can be worse than a thin film. Recently, anodized alumina templates have been used for the fabrication of WBG nanostructures, such as GaN nanowires arrays.[30] These studies indicate that emission characteristics of the GaN nanostructures are strongly influenced by the interactions with the anodic alumina membrane. These are in agreement with our expectations as anodic alumina provide a very strong bonding between GaN nanoislands and the passivation (Al_2O_3). The theoretical studies presented here suggest that bonding between the anodic alumina membrane and GaN enhance dislocation formation in the nanostructure and thus impact its optoelectronic properties.

In the previous sections, we developed a simplified mechanistic model to study dislocation nucleation in nanoislands. In this work only full edge dislocations were considered. (Other types, i.e., transverse, partial MDs, were not considered.) Dislocation reactions (i.e., annihilation, etc.) were ignored. Such an assumption has an impact, particularly in the high dislocation density region where the current model is likely to overestimate dislocation density. From an engineering perspective such an assumption is not troubling in the low dislocation density regime. Some interesting work in this regard has been presented by Mathis *et al.*[31] In this work dislocation energetics for the 3D nanoislands were formulated using superposition on the 2D dislocation energy model of Atkinson *et al.* for a rectangular stripe. However, rigorously, our dislocation energy results are strictly valid only for parallepiped geometries rather than smooth curved geometry of a cylinder. It is unlikely to have a major impact on our results though future work should focus on accurate dislocation energy calculation in smooth confined structures.

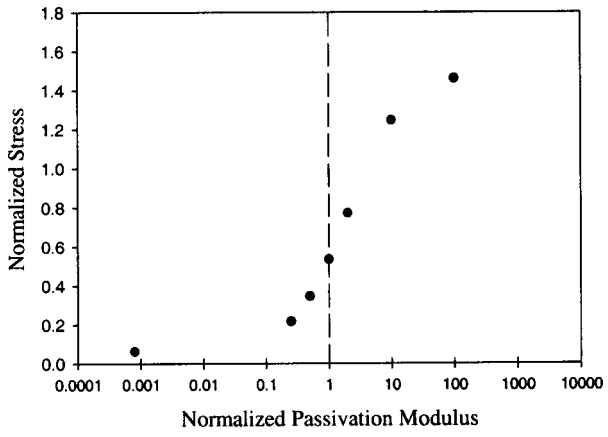

FIG. 6. Effect of passivation modulus on the normalized stress.

III. SIZE DEPENDENT SURFACE ELASTICITY IN WIDE BAND-GAP NANOSTRUCTURES

The size dependence of the band gap is one of the most remarkable aspects of quantum confinement in low dimensional systems. According to the phenomenological effective mass approximation, the increase in the band gap of a semiconductor quantum dot over its corresponding bulk value is inversely proportional to the square of the nanocrystal size.[32] In embedded quantum dots, elastic relaxation and the subsequent hydrostatic strain within the nanostructure, additionally, impact their bandgap and thus optoelectronic properties.[33,34] Accordingly, as a first approximation, the variation in the band gap of an embedded semiconductor spherical nanocrystal as a function of its size can be described as:

$$E_g = E_g(\text{bulk}) + \Delta E_g(\text{I}) + \Delta E_g(\text{II}), \tag{10}$$

$$\Delta E_g(\text{I}) = \frac{h^2\pi^2}{8\mu}\cdot\frac{1}{R^2} - \frac{1.8e^2}{\epsilon}\cdot\frac{1}{R}, \tag{10a}$$

$$\Delta E_g(\text{II}) = (a_c + a_v)\cdot\epsilon^T, \tag{10b}$$

where $\Delta E_g(\text{I})$ represents the quantum confinement effect and the Coulombic interaction. In Eq. (10a), $\mu=(1/m_e+1/m_h)^{-1}$ is the effective mass of holes and electrons, and ϵ is the dielectric constant of the semiconductor, and R is the radius of the nanocrystal. h and e represent the Planck constant and electron charge, respectively. $\Delta E_g(\text{II})$, in turn, represents the impact of the hydrostatic strain on the band gap of the nanocrystal. In Eq. (10b), a_c and a_v are the conduction and valence band deformation potential constants, while ϵ^T is the hydrostatic strain due to both the lattice mismatch between the quantum dot and the embedding matrix and the surface elasticity at the nanoscale (the latter being neglected in previous works). The quantum confinement effect has been investigated in great detail by numerous researchers and will not be further discussed in this article. We will only examine the influence of strain on the band gap of WBG semiconductor nanostructures, in particular the size dependent portion.

Existent analytical and numerical formulations of the strain state in embedded quantum dots are based on the conventional bulk elasticity.[33,34] Embedded dots can be treated as classical Eshelby inclusions with lattice mismatch strain as an eigenstrain. Solutions for such problems can be found

in standard texts. It has to be noted that classical elasticity does not admit intrinsic size dependence in the elastic solutions of inclusions and inhomogeneities. At the nanolength scale, however, size effects often become prominent; the causes of which need to be explicitly addressed. These may include higher order strain gradient and surface energy effects. We previously[35] demonstrated that higher order gradient effects are typically small as compared to the surface energy effects, and hence will be ignored in this work. In nanostructures with sizes below 50 nm, due to their high surface-to-volume ratios, strain energy can be dramatically altered compared to bulk due to surface/interface elasticity. Surface elasticity arises due to the deformation dependence of surface energy. In a small strain assumption, this dependence can be additively decomposed into a strain independent surface tension (τ_0) and a term that is linearly dependent on surface strain. The equilibrium and constitutive equations for isotropic case of a body with a surface/interface can be summarized as:[36]

In the bulk: $\sigma^B_{ij,j}=0; \quad \sigma^B_{ij}=\lambda\,\delta_{ij}\epsilon_{kk}+2\mu\epsilon_{ij}$

On the surface/interface: $\sigma^B_{\beta\alpha}n_\beta+\sigma^S_{\beta\alpha,\beta}=0;$

$$\sigma^B_{ji}n_jn_i=\sigma^S_{\alpha\beta}\kappa_{\alpha\beta}, \tag{11a}$$

$$\sigma^S_{\beta\alpha}=\tau_0\delta_{\beta\alpha}+2(\mu_s-\tau_0)\epsilon_{\beta\alpha}+(\lambda_s+\tau_0)\epsilon_{\gamma\gamma}\delta_{\beta\alpha}$$

where, λ and μ are the Lame' constants for the isotropic bulk material. Isotropic interfaces or surfaces can be characterized by surface Lame' constants λ^s, μ^s. Here, $\kappa_{\alpha\beta}$ represents the curvature tensor of the surface/interface, n_α is the normal vector on the interface. Where applicable, superscripts *B* and *S* indicate bulk and surface, respectively. It is to be noted that only certain strain components appear within the constitutive law for surfaces due to the 2×2 nature of the surface stress tensor (i.e., strains normal to the surface are excluded). Thus, the Greek indices take on values 1 and 2 while Latin subscripts adopt values 1 through 3. Using this formulation, recently Sharma *et al.*[36,37] derived a general expression for the radial strain, ϵ_{rr}, in embedded spherical quantum dots, including size dependent surface elasticity effects:

$$\epsilon_{rr}=\left(\frac{3K_I\epsilon^m-\dfrac{2\tau_0}{R}}{4\mu_M+3K_s+\dfrac{2K_s}{R}}\right), \tag{12}$$

where ϵ^m is the lattice mismatch, τ_0 is the surface or interfacial tension and K and μ are the bulk and shear modulus respectively. The subscripts *I* and *M* refer to the quantum dot and matrix, respectively. K_s is the surface modulus [$=2(\lambda_s+\mu_s)$]. Note that the mismatch strain must be subtracted from Eq. (12) before employing it in band structure calculations. Hence, the expression for total hydrostatic strain (including surface effects) for a spherical inclusion can be expressed as:

$$\epsilon^T=3\left(\frac{3K_I\epsilon^m-\dfrac{2\tau_0}{R}}{4\mu_M+3K_s+\dfrac{2K_s}{R}}-\epsilon_m\right). \tag{13}$$

Sharma *et al.*[35] have demonstrated that exclusion of size dependent surface elasticity can lead to as large as 12% errors in the estimation of strain in 2–10 nm InAs quantum dots embedded in a GaAs matrix.[36,37]

In this section, we will investigate size dependent strain effects in templated WBG nanostructures. Considering the nanoisland geometry of Fig. 1, the strain inside the WBG nanoisland is a combination of lattice mismatch with the underlying substrate/nucleation layer, ϵ^M, and surface effects, ϵ^S. Considering the effect of surface tension only, the result of strain for high aspect ratio nanoislands can be approximated as: $(\epsilon^M+\epsilon^S)$. Accordingly, for templated nanostructures, Eq. (10b) can be rewritten as:

$$\Delta E_g(\mathrm{II})=(a_c+a_v)\cdot\epsilon^T=(a_c+a_v)\cdot(\epsilon^M_{kk}+\epsilon^S_{kk}), \tag{14}$$

where, ϵ_{kk} represents the hydrostatic strain. It has to be noted that strain in templated nanoislands, such as in Fig. 1, is extremely inhomogeneous. A nonuniform strain typically requires solution of the fully coupled quantum eigenvalue problem to obtain the band gap. However, as a first approximation, a similar averaging scheme as for the dislocation nucleation can be applied. In contrast with the dislocation nucleation case, the averaging is done over the entire cylindrical geometry. Hence ϵ^M_{kk} can be expressed as:

$$\epsilon^M_{kk}=\epsilon^m\cdot\left\langle\overline{g\left(\frac{h}{R}\right)}\right\rangle. \tag{15}$$

The hydrostatic strain due to surface effects is given approximately by:

$$\epsilon^S_{kk}=2\cdot\frac{\tau_0}{K'_I\cdot R}, \tag{16}$$

where, K'_I is the effective bulk modulus in plane strain. The second-order effect due to surface elastic modulus K_s has been neglected. Hence the effect of strain on the band gap can be expressed as:

$$\Delta E_g(\mathrm{II})=(a_c+a_v)\cdot\epsilon^T$$
$$=(a_c+a_v)\cdot\left[\epsilon^m\cdot\left\langle\overline{g\left(\frac{h}{R}\right)}\right\rangle+2\cdot\frac{\tau_0}{K'_I\cdot R}\right]. \tag{17}$$

The expression developed in Eq. (17) is valid only for high aspect ratios (>3). It can be observed that while the effect of lattice mismatch is dependent only on the aspect ratio, the surface effect depends on the absolute size of the nanoisland. The surface effect becomes prominent when the radii are very small, i.e., in the nanometer range. We have used this formalism to calculate the size dependence in $\Delta E_g(\mathrm{II})$, Eq. (13), as a function of size for two WBG nanostructures, $In_{18}Ga_{82}N$, $In_{32}Ga_{68}N$. The nanostructures are supported on a GaN substrate and are surrounded by a weakly bound matrix (template), such as SiO_2. A cylindrical geometry is assumed for the nanoislands. The size indepen-

TABLE I. Constants and material properties used to calculated $\Delta E_g(\mathrm{II})$.

	E_g(Bulk) (eV)	ϵ^m	$\langle \overline{g}(h/R=5)\rangle$	$\langle \overline{g}(h/R=1)\rangle$	$\langle E\rangle^a$ (GPa)	ν^b
GaN	3.40	⋯	⋯	⋯	288.1	0.230
InN	0.70	⋯	⋯	⋯	143.9	0.330
$In_{18}Ga_{82}N$	2.47	0.0198	0.053	0.18	262.1	0.248
$In_{32}Ga_{78}N$	1.94	0.0349	0.050	0.19	242.0	0.262

[a] $\langle E\rangle = E(\mathrm{GaN})\cdot x + E(\mathrm{InN})\cdot(1-x)$, where x is the In fraction in the compound.
[b] $\nu = 0.23 + 0.1\cdot x$ (Ref. 41).

dent parameters $\langle \overline{g}(h/R)\rangle$ are estimated for each WBG as a function of their composition and aspect ratio. In Table I, $\langle \overline{g}(h/R)\rangle$ and other parameters and constants used for the calculation of $\Delta E_g(\mathrm{II})$ for the two WBG nanostructures are collected. We have assumed that τ_0 is equal to 1.9 N/m (Ref. 38) and is composition independent. Finally, $(a_c + a_v)$ for these WBG is equal to 8.3 eV.[39] In Fig. 7 the variation of $\Delta E_g(\mathrm{II})$ as a function of size is illustrated for templated $In_{32}Ga_{68}N$ nanorods (cylinders) with an aspect ratio of 5. In this figure, we have also included the case of $In_{32}Ga_{68}N$ spherical quantum dots embedded in a GaN matrix for comparison purposes. It should be noted that in contrast with the templated configuration, strain in embedded nanoclusters is uniform. In addition, different expressions for K_I' are used to reflect the specific geometry of the nanostructure.[40] As mentioned earlier, $\Delta E_g(\mathrm{II})$ is a combination of both mismatch strain and surface elasticity induced variations in the band gap. *Strain induced effects* result in a vertical shift of $\Delta E_g(\mathrm{II})$ along the y axis. Spherical $In_{32}Ga_{68}N$ quantum dots embedded in a GaN matrix experience a larger mismatch strain as compared to the templated nanoislands (see Fig. 7). In templated structures, lattice mismatch induced strain effects become less significant with increasing the aspect ratio of the cylindrical nanoislands. *Surface elasticity induced effects* result in size dependency of the $\Delta E_g(\mathrm{II})$, thus accounting for the curvature of the $\Delta E_g(\mathrm{II})$ plots. As can be seen in Fig. 7, below 10 nm, $\Delta E_g(\mathrm{II})$ abruptly increases with size, regardless of the geometry of the nanostructure. In Fig. 8, the variation of $\Delta E_g(\mathrm{II})$ as a function of size is plotted for relatively high aspect ratio $(h/R=5)$ $In_{18}Ga_{82}N$, $In_{32}Ga_{68}N$ nanorods. As mentioned earlier, misfit induced strain effects are

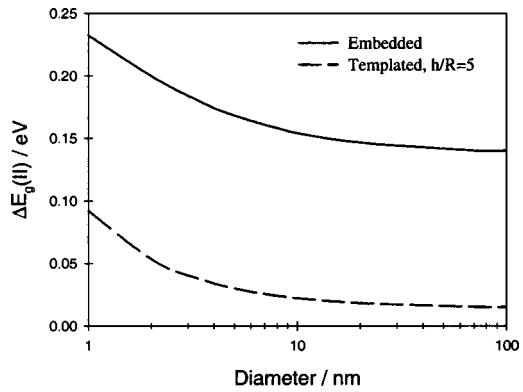

FIG. 7. Variation of $\Delta E_g(\mathrm{II})$ as a function of size in $In_{32}Ga_{68}N$ nanorods of varying aspect ratio (h/R).

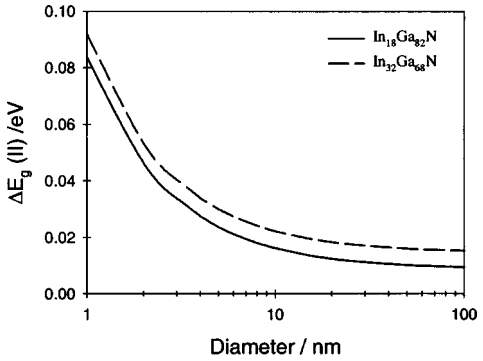

FIG. 8. Variation of $\Delta E_g(\mathrm{II})$ as a function of size for high aspect ratio nanoislands.

rather negligible for high aspect ratio templated nanoislands. Therefore, the variation of $\Delta E_g(\mathrm{II})$ in templated high aspect ratio nanoislands is mostly due to the surface elasticity effects. The variations in band gap due to surface elasticity effects reported here could be as large as 20–100 meV. It should be noted that in optical applications, even variations on the order of 10 meV are considered large and in some instances intolerable. These surface elasticity effects can be further exploited in a variety of applications, such as in optoelectronics and biochemical sensing. The results presented here highlight the importance of coupling the surface elasticity and quantum effects. It must be noted that the nanoscale structures are neither isotropic nor cylindrical. Experimental values for surface moduli and surface tension are rarely available. Nevertheless, our preliminary work points to some interesting physical effects. To expand the scope and validity of this work, we are employing numerical density functional theory approaches. These studies will be reported in a future publication.

IV. CONCLUSIONS

A mechanistic model for misfit dislocation nucleation and dislocation density calculation for 3D confined geometries is developed in this article. Some of the major implications are that nanoscale 3D confinement of epitaxial semiconductor films can result in extremely low dislocation densities in contrast to 2D confinement. Intuitively, passivation material has a detrimental impact on the defect state of nanoislands. It is advantageous to have either a weakly bonded passivation or alternatively a compliant material with very low elastic modulus (the best case scenario being where no passivation is present). Interestingly, in cases of very rigid passivation or extremely strong bonding, the stress state in nanoislands can be worse than that of a thin film!

In the present work, size dependency of strain in templated WBG nanostructures has been discussed. The size dependency of strain is caused by the distinct elastic behavior of surfaces and interfaces at the nanoscale as compared to the bulk. Surface strains appear to be only influential in the nanometer regime (<10 nm) due to appreciable surface-to-volume ratios. The results presented here suggest that the optoelectronic properties of templated WBG nanostructures can be significantly affected by size dependent strains. In

particular, for high aspect ratio templated nanorods, errors as large as 100 meV in band-gap prediction can occur if the size dependency of strain is ignored.

ACKNOWLEDGMENTS

Support from M. L. Blohm and the Nanotechnology Program at GE Global Research Center are appreciated.

[1] A. P. Alivasatos, Science **271**, 933 (1996).
[2] D. Bimberg, M. Grundmann, and N. N. Lendenstov, in *Quantum Dot Heterostructures* (Wiley, New York, 1996).
[3] Y. Arakawa, IEEE J. Sel. Top. Quantum Electron. **8**, 823 (2002).
[4] S. Nakamura, S. Pearton, and G. Fasol, *The Blue Laser Diode: The Complete Story* (Springer, Berlin, 2000).
[5] Y. Huang, Y. C. Duan, and C. M. Leiber, Nano Lett. **2**, 101 (2002).
[6] Y. Arakawa and H. Sakaki, Appl. Phys. Lett. **40**, 939 (1982); B. Damilano, N. Grandjean, F. Semond, and L. M. Massies, *ibid.* **75**, 962 (1999).
[7] S. Chichibu, T. Azuhata, T. Sota, and S. Nakamura, Appl. Phys. Lett. **69**, 4188 (1996).
[8] Y. Nakamura, Y. Kawakami, M. Funato, S. Fujita, S. Fujita, and S. Nakamura, Appl. Phys. Lett. **70**, 981 (1997).
[9] X. Duan, Y. Huang, Y. Cui, and C. M. Leiber, J. Am. Chem. Soc. **122**, 188 (2000).
[10] H. M. Kim, T. W. Kang, and K. S. Chung, Adv. Mater. (Weinheim, Ger.) **15**, 567 (2003).
[11] O. I. Micic, S. P. Ahrenkiel, D. Bertram, and A. J. Nozik, Appl. Phys. Lett. **75**, 478 (1999).
[12] M. Kuball, M. Benyoucef, F. H. Morrisrey, and C. T. Foxon, MRS Internet J. Nitride Semicond. Res. **5s1**, (2000).
[13] H. Mohseni, Ph.D. thesis, Northwestern University, 2001; Razeghi *et al.* http://cqd.ece.northwestern.edu/
[14] S. Tanaka, S. Iwai, and Y. Aoyagi, Appl. Phys. Lett. **69**, 4096 (1996).
[15] S. Tanaka, H. Hirayama, and Y. Aoyagi, Appl. Phys. Lett. **71**, 1299 (1997).
[16] O. Moriwaki, T. Somaya, K. Tachibana, S. Ishida, and Y. Arakawa, Appl. Phys. Lett. **76**, 2361 (2000).
[17] C. Norenberg, R. A. Oliver, M. G. Martin, L. Allers, M. R. Castel, and G. A. Briggs, Phys. Status Solidi A **194**, 536 (2002).
[18] K. Tachibana, T. Someya, S. Ishida, and Y. Arakawa, J. Cryst. Growth **237**, 1312 (2002); K. Tachibana, T. Someya, I. Satomi, and Y. Arakawa, Appl. Phys. Lett. **76**, 3212 (2000).
[19] K. Kawasaki, I. Nakamatsu, H. Hirayama, K. Tsutsui, and Y. Aoyagi, J. Cryst. Growth **243**, 129 (2002).
[20] I. A. Ovid'ko, Rev. Adv. Mater. Sci. **1**, 61 (2000).
[21] L. B. Freund, MRS Bull. **17**, 52 (1992).
[22] A. Atkinson and S. C. Jain, J. Appl. Phys. **72**, 2242 (1992).
[23] S. C. Jain, A. H. Harker, A. Atkinson, and K. Pinardi, J. Appl. Phys. **78**, 1630 (1995).
[24] A. Atkinson, S. C. Jain, and A. H. Harker, J. Appl. Phys. **77**, 1907 (1995); A. Atkinson, K. Pinardi, and S. C. Jain, Semicond. Sci. Technol. **11**, 1271 (1996).
[25] J. R. Downes, D. J. Dunstan, and D. A. Faux, Philos. Mag. Lett. **76**, 77 (1997); A. D. Andreev, J. R. Downes, D. A. Faux, and E. P. O'Reilly, J. Appl. Phys. **86**, 297 (1999).
[26] I. A. Ovid'ko and A. G. Sheinerman, Appl. Phys. A: Mater. Sci. Process. **74**, 273 (2002); I. A. Ovid'ko, Phys. Rev. Lett. **88**, 046103 (2002).
[27] S. Luryi and E. Suhir, Appl. Phys. Lett. **49**, 140 (1986).
[28] C. Kim, I. K. Robinson, J. Myoing, K. Shim, M.-C. Yoo, and K. Kim, Appl. Phys. Lett. **69**, 2358 (1996); J. W. Matthews and A. E. Blakeslee, J. Cryst. Growth **32**, 265 (1974); A. Fischer, H. Kuhne, and H. Richter, Phys. Rev. Lett. **73**, 2712 (1994).
[29] L. W. Tu, C. L. Hsiao, T. W. Chi, I. Lo, and K. Y. Hsieh, Appl. Phys. Lett. **82**, 1601 (2003).
[30] J. Zhang, L. D. Zhang, X. F. Wang, C. H. Liang, X. S. Peng, and Y. W. Wang, J. Chem. Phys. **115**, 5714 (2001); G. S. Cheng, L. D. Zhang, X. G. Zhu, S. H. Chen, Y. Li, Y. Zhu, and G. T. Fei, Nanostruct. Mater. **11**, 421 (1999).
[31] S. K. Mathis, A. E. Romanov, L. F. Chen, G. E. Beltz, W. Pompe, and J. S. Speck, J. Cryst. Growth **231**, 371 (2001).
[32] L. E. Brus, J. Chem. Phys. **80**, 4403 (1984).
[33] A. J. Williamson and A. Zunger, Phys. Rev. B **58**, 6724 (1998).
[34] M. Grundman, O. Stier, and D. Bimberg, Phys. Rev. B **52**, 11969 (1995).
[35] P. Sharma, S. Ganti, H. Ardebili, and A. Alizadeh, J. Appl. Phys. **95**, 2763 (2004).
[36] P. Sharma and S. Ganti, Phys. Status Solidi B **234**, R10 (2002).
[37] P. Sharma, S. Ganti, and N. Bhate, Appl. Phys. Lett. **82**, 535 (2003).
[38] J. E. Northrup and J. Neugebauer, Phys. Rev. B **53**, R10477 (1996).
[39] V. E. L. Chin, T. L. Tansley, and T. Osotchan, J. Appl. Phys. **75**, 7365 (1994).
[40] For nanoislands with a cylindrical morphology, $K_I = 2\lambda + 2\mu$. For spherical nanostructures, on the other hand, $K_I = \lambda + 2/3\mu$. λ and μ in turn are the Lame constants and can be easily calculated from the modulus and Poisson ratio values provided in Table I.
[41] T. Takeuschi, H. Takeuchi, S. Sota, H. Sakai, H. Amano, and I. Akasaki, Jpn. J. Appl. Phys., Part 2 **36**, L177 (1997).